Phase Transition Properties of 3D Potts Models

Alexei Bazavov[a], Bernd A. Berg[b,c] and Santosh Dubey[b,c]

[a)] *Department of Physics, University of Arizona, Tucson, AZ 85721, USA*

[b)] *Department of Physics, Florida State University, Tallahassee, FL 32306, USA*

[c)] *School of Computational Science, Florida State University, Tallahassee, FL 32306, USA*

(Dated: April 8, 2008)

Using multicanonical Metropolis simulations we estimate phase transition properties of 3D Potts models for $q = 4$ to 10: The transition temperatures, latent heats, entropy gaps, normalized entropies at the disordered and ordered endpoints, interfacial tensions, and spinodal endpoints.

I. INTRODUCTION

Potts models were introduced as a footnote in the thesis by Potts [1] on clock models, whose investigation had been proposed to him by his adviser Domb. We define their energy function by

$$E^{(k)} = 2 \sum_{\langle ij \rangle} \left(\frac{1}{q} - \delta(q_i^{(k)}, q_j^{(k)}) \right) \tag{1}$$

where $\delta(q_i, q_j)$ is the Kronecker delta function, the sum $\langle ij \rangle$ is over the nearest neighbor lattice sites, the index (k) refers to the configuration, and $q_i^{(k)}$ is the Potts spin at site i. For the q-state model Potts spins take the values $0, 1, \ldots, q-1$. Following the notation of Ref. [2] the factor of two in front of the sum is introduced to match for $q = 2$ on Ising model conventions. Expectation values of the Gibbs canonical ensemble are calculated with the Boltzmann (or Gibbs) factor $\exp(-\beta E)$, $\beta = 1/(kT)$.

Potts, and not so much clock models, received considerable attention up to the day. Developments till 1982 were reviewed by Wu [3]. In 2D the models have second order phase transitions for $q = 2$ to 4, and first order transitions for $q \geq 5$. In a work by Baxter [4], critical temperatures, latent heats and entropies were analytically derived. Equations for interface tensions followed later [5] and played a role in the verification of the multicanonical approach [6] to Markov Chain Monte Carlo (MCMC) simulations. In 3D the $q = 2$ Ising model phase transition is second and the $q \geq 3$ transitions are first order. The strength of the first order transitions, measured by their latent heat, increases with q. The $q = 5$ transition in 2D and the $q = 3$ transition in 3D are weakly first order.

Potts models proved amazingly versatile to grasp the essence of physically interesting

situations, many of them are described in Ref. [3]. When they are generalized by introducing quenched random variables as exchange constants, the Ising case of the Edwards-Anderson spin glass [7] and quadrupolar Potts glasses [8] are obtained. Particular choices give antiferromagnets and the fully frustrated Ising model [9].

The 3D $q = 3$ Potts model shares the center symmetry of SU(3) gauge theory [10] and plays a role in our understanding of the QCD deconfining phase transition. This and other motivations led to a number of numerical investigations of the 3D 3-state Potts model [11, 12, 13, 14, 15, 16, 17, 18]. However, when we recently looked out for a strong first order transition in 3D, we found only a few papers [19, 20, 21] dealing with 3D Potts for $q \geq 4$. The purpose of this paper is to fill this gap in the literature for 3D Potts models up to $q = 10$. Thereby, we will closely follow the outline of a previous investigation of the equilibrium statistical properties of the 3D 3-state Potts model by two of the present authors [18].

Next, we briefly summarize our simulation method and give an overview of our assembled statistics. In section III we calculate and analyze transition temperatures, specific and latent heats. Section IV deals with entropy and energy across the phase transition, section V with interface tensions and spinodal endpoints. A brief summary and conclusions are given in the final section VI.

II. SIMULATION METHOD AND OVERVIEW OF DATA

We want to calculate expectation values $\mathcal{O}$ in the Gibbs canonical ensemble. They are given by the ensemble average

$$\widehat{\mathcal{O}} = \widehat{\mathcal{O}}(\beta) = \langle \mathcal{O} \rangle_\beta = Z^{-1} \sum_{k=1}^{K} \mathcal{O}^{(k)} \, e^{-\beta \, E^{(k)}} \tag{2}$$

where

$$Z = Z(\beta) = \sum_{k=1}^{K} e^{-\beta \, E^{(k)}} = \sum_{E} n(E) \, e^{-\beta \, E} \tag{3}$$

is the partition function. The index (k), $k = 1, \ldots, K$ labels the configurations (microstates) of the system and $E^{(k)}$ is the (internal) energy of configuration (k). In the last equation $n(E)$ is the number of configurations with energy E.

We consider Potts models on cubic lattices of size L^3 with periodic boundary conditions. There are $N = L^3$ Potts spins. Each microstate k defines a unique arrangement of Potts spins and vice versa:

$$k = \{q_1^{(k)}, \ldots, q_N^{(k)}\} \; . \tag{4}$$

As each Potts spin can take on q values, there are

$$K_L = Z_L(0) = \sum_E n_L(E) = q^N \ , \tag{5}$$

microstates. Even for rather small numbers of L, K is a very large, so that one will not be able to sum the partition function explicitly. Instead, one can use statistical methods.

MCMC simulations [2] are a suitable approach to evaluate equilibrium properties of the canonical ensemble. Off the phase transition temperatures canonical Metropolis or heatbath simulations with weight factor $\exp(-\beta E)$ work sufficiently well, provided a ordered start is used for simulations in the ordered phase, and (somewhat less important) a disordered start for simulations in the disordered phase. However, canonical simulations deteriorate quickly when it comes to the (most interesting) investigation of phase transition properties. For first order transitions the reason is that the relevant transition states are in the canonical ensemble suppressed $\sim \exp(-2\sigma_{od}\, L^{D-1})$, where σ_{od} is the order-disorder interface tension.

Multicanonical simulations [2, 6] are a remedy for this supercritical slowing down. One performs for $E_{\rm min} \le E \le E_{\rm max}$ MCMC simulations with a working approximation of the weight factors

$$w_{\rm muca}(E) = e^{-b(E)\,E + a(E)} = \frac{1}{n(E)} \, , \tag{6}$$

supplemented by the canonical weights $\exp(-\beta_{\rm max} E)$ for $E < E_{\rm min}$ and $\exp(-\beta_{\rm min} E)$ for $E > E_{\rm max}$. Here $n(E)$ is the number of states with energy E as introduced by Eq. (3). With the weights (6) all energies in the range $E_{\rm min} \le E \le E_{\rm max}$ are sampled with the same probability, so that the Markov process will perform some kind of random walk in the range $E_{\rm min} \le E \le E_{\rm max}$. The microcanonical inverse temperature $b(E)$ and the dimensionless free energy $a(E)$ follow uniquely from $n(E)$ due to the relation

$$a(E-\epsilon) = a(E) + [b(E-\epsilon) - b(E)]\ E \, , \quad a(E_{\rm max}) = 0 \, , \tag{7}$$

where ϵ is the step to the next energy. However, $n(E)$ is a-priori unknown, so that some iterative procedure needs to be used. In this context working approximation of the weights means that any weights that enable cycling (also called tunneling)

$$E_{\rm max} \ \rightarrow \ E_{\rm min} \quad \text{and} \quad \text{back} \tag{8}$$

are considered to be acceptable. Actually it is known that not the weights (6), but some modifications of them, can be optimal for that purpose [22, 23] and it should be noted that there is a residual exponential slowing down [24].

We find working estimates of the multicanonical weights by finite size (FS) extrapolations from a smaller lattice to a next larger lattice, a method which was already used in [6]. Obviously, this requires that the FS behavior of the system under consideration is well

defined. In particular, for complex systems like spin glasses or proteins this is not the case and more sophisticated recursion approaches need to be used [2], most noted is presumably the one by Wang and Landau [25].

Let $e = E/N = E/L^3$ be the energy density. For our Potts models we simply convert the microcanonical inverse temperature $b_{L_1}(E)$ for a given lattice size L_1 to the $b_{L_2}(E)$ of our next larger lattice size $L_2 > L_1$ via the interpolation

$$b_{L_2}(E) = w_+ \, b_{L_1}(E_+) + w_- \, b_{L_1}(E_-) \quad \text{with} \quad w_\pm = \frac{|e - e_\mp|}{e_+ - e_-} \; , \tag{9}$$

where $e = E/(L_2)^3$ and $e_- < e$ and $e_+ > e$ are the values closest to e, so that we have for the corresponding E_+ and E_- values entries in $b_{L_1}(E)$. For our purposes this simple procedure turned out to be sufficiently accurate. Better extrapolations can be expected by taking into account details of the shape of $n_L(E)$, as for a magnetic field driven phase transition discussed in Ref. [26].

Suitably, the $E_{\rm max}$, $E_{\rm min}$, $\beta_{\rm min}$ and $\beta_{\rm max}$ parameters, which accompany the weights (6) are chosen so that they embrace the phase transitions and that

$$E_{\rm max} = \langle E \rangle_{\beta_{\rm min}} \; , \qquad E_{\rm min} = \langle E \rangle_{\beta_{\rm max}} \tag{10}$$

holds. From a simulation with these weights, canonical expectation values are obtained by reweighting for the temperature range $\beta_{\rm min} \leq \beta \leq \beta_{\rm max}$. This property has coined the name multicanonical. To calculate the partition function (3), from which the normalized entropy and free energy follow, one has to include $\beta = 0$ in this temperature range. So we choose $\beta_{\rm min} = 0$, for which our normalization of the energy (1) implies $E_{\rm max} = 0$. For $\beta_{\rm max}$ we chose the values given in table I, each of them well above the transition value β_c. Our simulations of multicanonical ensembles defined by the weights (6) rely on the Metropolis algorithm. We update sequentially with one Metropolis update per spin during one sweep through the lattice. This is more efficient [2] than picking spins at random for the updates.

In table I we give an overview of the statistics per run. We followed the outline of Potts model MCMC simulations in [2]. First, we performed the number of sweeps listed in table I for reaching equilibrium. Data from these sweeps are excluded from the statistics for which measurements were performed. Subsequently, we collected for each run 32 histograms, each relying on the number of sweeps listed in the table. All error bars are then calculated with respect to these 32 bins (32 jackknife bins when nonlinear operations on the data are involved). From the student distribution it is known that error bars from 32 independent Gaussian data give almost Gaussian confidence probabilities at the level of two standard deviations.

For most data points we performed two runs with the statistics of table I. The first runs are based on the weights iterated from the closest smaller lattice. These data are taken

TABLE I: Analyzed statistics per production run in sweeps: 32 × the number given.

L	$q=4$	$q=5$	$q=6$	$q=7$	$q=8$	$q=9$	$q=10$
$\beta_{\max}=$	0.45	0.41	0.43	0.45	0.47	0.49	0.50
2	256	1024	6×10^3	10×10^3	15×10^3	15×10^3	16384
3	1024	2048	9×10^3	10×10^3	15×10^3	15×10^3	4000
4	1024	2048	9×10^3	10×10^3	20×10^3	20×10^3	4000
6	4096	8192	1×10^4	15×10^3	20×10^3	30×10^3	65536
8	4096	32768	4×10^4	45×10^3	5×10^4	75×10^3	262144
10	16384	10×10^4	16×10^4	25×10^4	3×10^5	4×10^5	1048576
12	65536	25×10^4	3×10^5	45×10^4	55×10^4	7×10^5	4194304
14	262144	45×10^4	5×10^5	14×10^5	17×10^5	22×10^5	16777216
16	262144	85×10^4	15×10^5	20×10^5	26×10^5	32×10^5	2×10^7
18	1048576	13×10^5	21×10^5	29×10^5	70×10^5	2×10^7	4×10^7
20	4194304	19×10^5	30×10^5	50×10^5	14×10^6	8×10^7	8×10^7
22	–	–	–	1×10^7	3×10^7	–	–
24	45×10^5	39×10^5	1×10^7	3×10^7	–	–	–
26	9×10^6	–	2×10^7	–	–	–	–
28	14×10^6	1×10^7	–	–	–	–	–
30	15×10^6	3×10^7	–	–	–	–	–

to refine the weights for the lattices at hand. The refined weights are used for the second production runs on these lattices. Exceptions from this procedure are iterations from a smaller to a larger lattice immediately after the first run. This speeds up the process of getting to larger lattices and has often been done when the cycling frequency of the first run was already satisfactory.

Table II collects the number of cycling (8) events obtained in the first production runs. For $L=2$, some cycling is already achieved by a canonical simulation at $\beta=0$. This allows one to determine multicanonical weights for the second run on 2^3 lattices, which have large cycling rates as shown in table III, and to start off FS iterations of the weights. From the 2^3 lattices we extrapolate weights for the first runs on 3^3 lattices, refine them for the second runs on 3^3 lattices, iterate to the next larger lattice, and so on (up to the before mentioned exceptions). The calculations were carried out on PC clusters at FSU. Our present lattice

TABLE II: Number of cycling events for the first production runs.

	$q=4$	$q=5$	$q=6$	$q=7$	$q=8$	$q=9$	$q=10$
$L=\ 2:$	3	6	4	2	1	1	1
$L=\ 3:$	32	135	350	246	239	104	15
$L=\ 4:$	109	139	377	358	550	531	88
$L=\ 6:$	68	117	80	98	89	87	164
$L=\ 8:$	21	125	106	76	71	92	113
$L=10:$	20	186	190	189	122	109	135
$L=12:$	77	249	195	169	99	52	107
$L=14:$	173	279	178	242	102	42	86
$L=16:$	125	313	301	139	47	12	11
$L=18:$	353	322	228	69	38	10	3
$L=20:$	711	327	172	48	11	5	2
$L=22:$	–	–	–	27	6	–	–
$L=24:$	441	84	1	27	–	–	–
$L=26:$	903	–	116	–	–	–	–
$L=28:$	867	43	–	–	–	–	–
$L=30:$	356	639	–	–	–	–	–

sizes are limited by the deterioration of cycling with increasing L, the computational power of a single PC (here 2-3 GHz per PC), and the limitation of the total length of one run to a few months.

During the simulations we collect histograms of the energy in the multicanonical ensemble, $h_{mu}(E)$, and calculate functions of the energy $f(E)$ from them by reweighting to the canonical ensemble:

$$\overline{f} = \frac{\sum_E f(E)\, h_{mu}(E)\, \exp\left[-\beta\, E + b(E)\, E - a(E)\right]}{\sum_E h_{mu}(E)\, \exp\left[-\beta\, E + b(E)\, E - a(E)\right]}\ , \tag{11}$$

where the sums are over all energy values for which $h_{mu}(E)$ has entries. The computer implementation of this equation requires care, because the differences between the largest and the smallest numbers encountered in the exponents can be large. We rely here on the logarithmic coding of Ref. [2]. Whenever the function $f(E)$ is non-linear jackknife binning is employed.

TABLE III: Number of cycling events for the second production runs.

	$q=4$	$q=5$	$q=6$	$q=7$	$q=8$	$q=9$	$q=10$
$L=\ 2:$	139	1451	5918	7091	2614	7985	6339
$L=\ 3:$	288	378	1275	1167	1436	1209	1098
$L=\ 4:$	72	126	410	331	578	497	324
$L=\ 6:$	69	100	109	127	117	165	311
$L=\ 8:$	22	154	125	117	105	110	349
$L=10:$	42	180	223	295	243	273	598
$L=12:$	93	256	221	228	218	246	1142
$L=14:$	209	251	219	427	384	394	2423
$L=16:$	130	308	366	396	352	359	1542
$L=18:$	323	301	347	342	585	1056	1707
$L=20:$	921	307	329	358	590	2168	1591
$L=22:$	–	–	–	405	779	–	–
$L=24:$	521	321	487	910	–	–	–
$L=26:$	–	–	708	–	–	–	–
$L=28:$	986	460	–	–	–	–	–
$L=30:$	869	–	–	–	–	–	–

III. ENERGIES, TRANSITION TEMPERATURES AND LATENT HEATS

In Fig. 1 we show internal energies as functions of β, for each q from the largest available lattice (error bars are not resolved on the scale of this figure). This gives a rough estimate of the latent heats and the inverse transition temperatures β_t. Accurate results follow from FS extrapolations of indicators, which are defined on finite lattices, so that they converge in the limit $L \to \infty$ (quickly) towards the infinite volume value of the desired physical quantity.

We calculate specific heats via the fluctuation-dissipation theorem

$$C = \frac{(\beta)^2}{L^3} \left(\langle E^2 \rangle - \langle E \rangle^2 \right) \ . \tag{12}$$

For first order phase transitions the finite volume specific heats are regularization of Dirac delta functions, which are the infinite volume extrapolations. The multicanonical approach allows to calculate specific heat values for a continuous range of β values. Consequently, the locations of the maxima can be accurately determined.

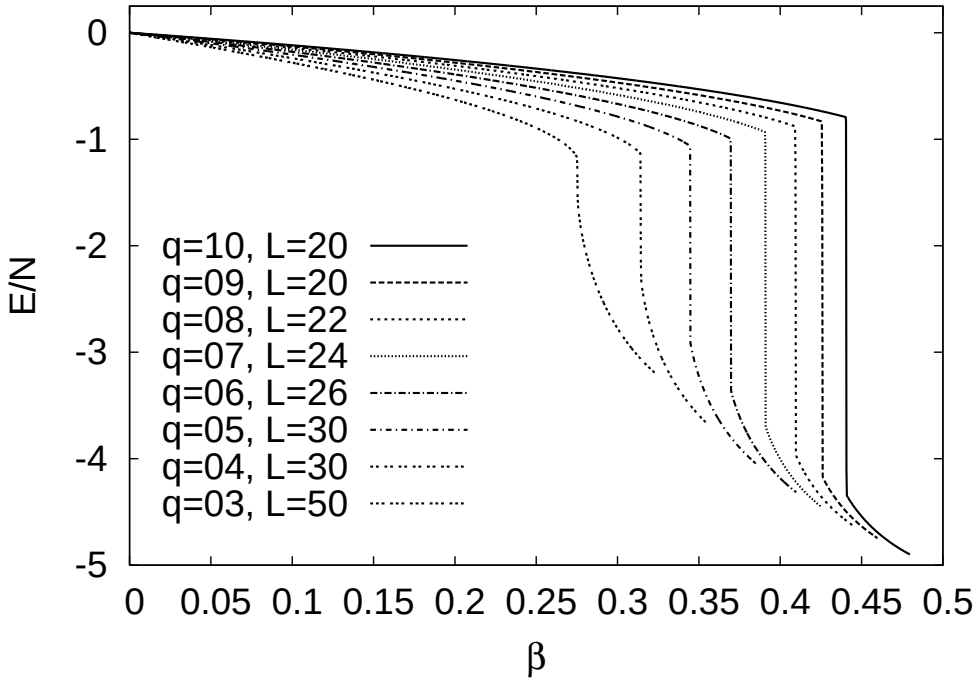

FIG. 1: Internal energies.

Finite lattice indicators for the transition temperatures are called pseudo transition temperatures, and there are various options to define them. On finite volumes their values differ, while they all converge to the same $L \to \infty$ limit. We use here three definitions of pseudo transition temperatures: β_{pt}^1, the β value at which equal heights are achieved in the double peaked energy histogram, β_{pt}^2, the position of the central energy of the latent heat, and β_{pt}^3, the location of the maximum of the specific heat. The first two definitions are explained in more detail later, β_{pt}^2 plays a role in determining the entropy gaps in section IV and β_{pt}^1 for the interface tensions in section V (they are labeled in this order for consistency with Ref. [18]).

For $q = 4$ Fig. 2 shows our linear fits

$$\beta_{pt}^i(L) = \beta_t^i + \frac{c^i}{L^3} \ , \tag{13}$$

which determine the infinite volume transition temperatures. The vertical order of the fits agrees with that in the legend. While the finite volume estimators $\beta_{pt}^i(L)$ differ, the infinite volume extrapolations are consistent with one another. The smallest lattices have been omitted from the fits to ensure an acceptable goodness of fit Q [2] in each case. This $q = 4$ pattern repeats for all q: The quality of the fits from our three definitions of pseudo transitions temperatures are similar, and the final estimates as well as their error bars are

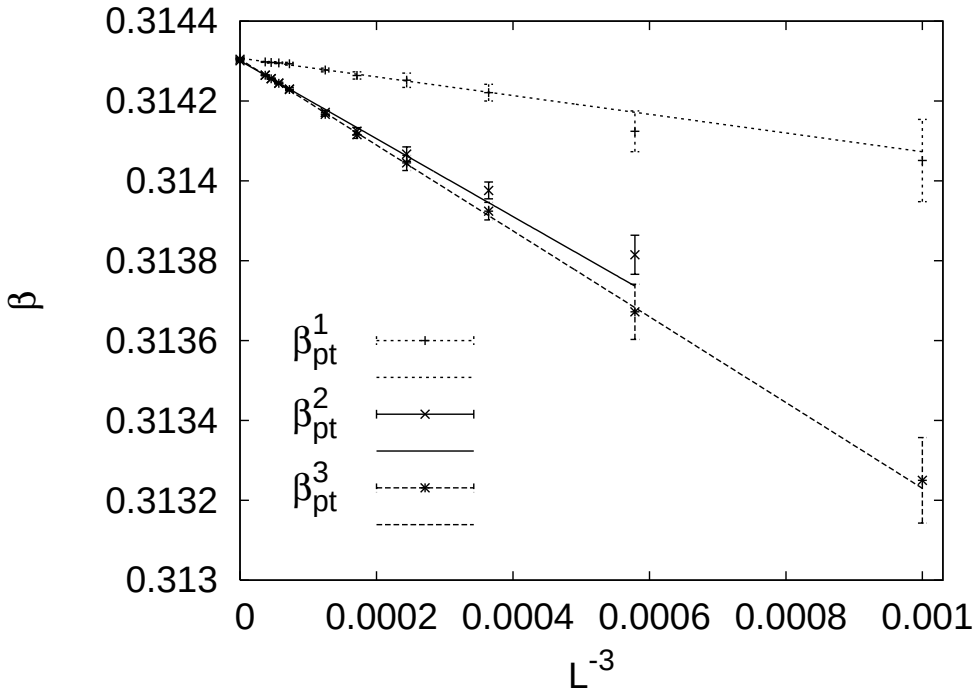

FIG. 2: Transition temperature fits for $q = 4$.

consistent with one another. To give one best number for each q, we simply average over the three estimates. We average also their error bars, because all three estimators rely on the same simulation, so that one does not expect error bar reduction when averaging over them. The thus obtained transition values $\beta_t(q)$ are collected in table IV. For the convenience of the reader we have included $q = 3$ and 2 estimates from Ref. [18] and [27], respectively. So far we have not found a simple formula for the q dependence like $\beta_t = \ln(1 + \sqrt{q})/2$, which holds in 2D [4] (given here in our convention).

Following Ref. [28], we extract the latent heat $\triangle e = \triangle E/N$ by fitting the maxima of the specific heat to the form

$$C_{\max}(L) = a_1 + a_2\, L^3 \tag{14}$$

and using the relation

$$a_2 = \frac{1}{2}\,(\beta_t)^2\,(\triangle e)^2\ . \tag{15}$$

The results are also included in table IV.

IV. ENTROPY AND ENERGY ACROSS THE PHASE TRANSITIONS

The entropy density is

$$s = \beta\,(e - f)\ , \tag{16}$$

TABLE IV: Estimates of observables ($q = 2$ from Ref. [27] and $q = 3$ from Ref. [18]).

q	β_t	$\triangle e$	$e(\beta_t)$	e^+	e^-
2	0.2216544 (06)	0	-0.9957 (14)	$e(\beta_t)$	$e(\beta_t)$
3	0.2752827 (29)	0.3286 (15)	-1.3470 (74)	-1.1826 (73)	-1.5112 (79)
4	0.3143041 (17)	1.16294 (61)	-1.719 (36)	-1.1367 (64)	-2.3019 (64)
5	0.3447205 (12)	1.84619 (20)	-1.987 (20)	-1.063 (20)	-2.910 (20)
6	0.3697070 (15)	2.36442 (17)	-2.177 (26)	-0.995 (26)	-3.359 (26)
7	0.3909657 (17)	2.76430 (12)	-2.316 (22)	-0.934 (22)	-3.698 (22)
8	0.4094959 (23)	3.08039 (15)	-2.421 (32)	-0.881 (32)	-3.961 (32)
9	0.4259432 (23)	3.33628 (12)	-2.503 (32)	-0.835 (32)	-4.171(32)
10	0.4407371 (18)	3.547570 (87)	-2.567 (25)	-0.794 (25)	-4.341 (25)

where f is the free energy density, which is continuous at the phase transition. So, the entropy gaps across the phase transitions are

$$\triangle s = \beta_t \, \Delta e \, , \tag{17}$$

or $\triangle s = 2\sqrt{a_2}$ with a_2 from the fits (14). The entropy and energy density endpoints in the disordered (+) and ordered (−) phases are given by

$$s^+ \;=\; \beta_t \, (e^+ - f(\beta_t)) \, , \tag{18}$$

$$s^- \;=\; \beta_t \, (e^- - f(\beta_t)) \, , \tag{19}$$

and are more difficult to compute than the gaps, because the additive normalization constants no longer drop out. We follow the method of Ref. [18], which relies on the definition of β_{pt}^2 as given below.

In multicanonical simulations, the normalization constant for the entropy is determined by the known value at $\beta = 0$:

$$S_0 = \ln \left(q^N \right) \quad \text{and} \quad s_0 = \frac{S_0}{N} = \ln q \; . \tag{20}$$

Fig. 3 shows normalized entropy densities of our models for our largest lattices.

To calculate the endpoints of the entropy and energy on the ordered and disordered sides of the transitions, we define $\beta_{pt}^2(L)$ by the relation

$$e_L(\beta_{pt}^2) = \frac{1}{2} \, \left[e_L^+(\beta_{pt}^2) + e_L^-(\beta_{pt}^2) \right] \, , \tag{21}$$

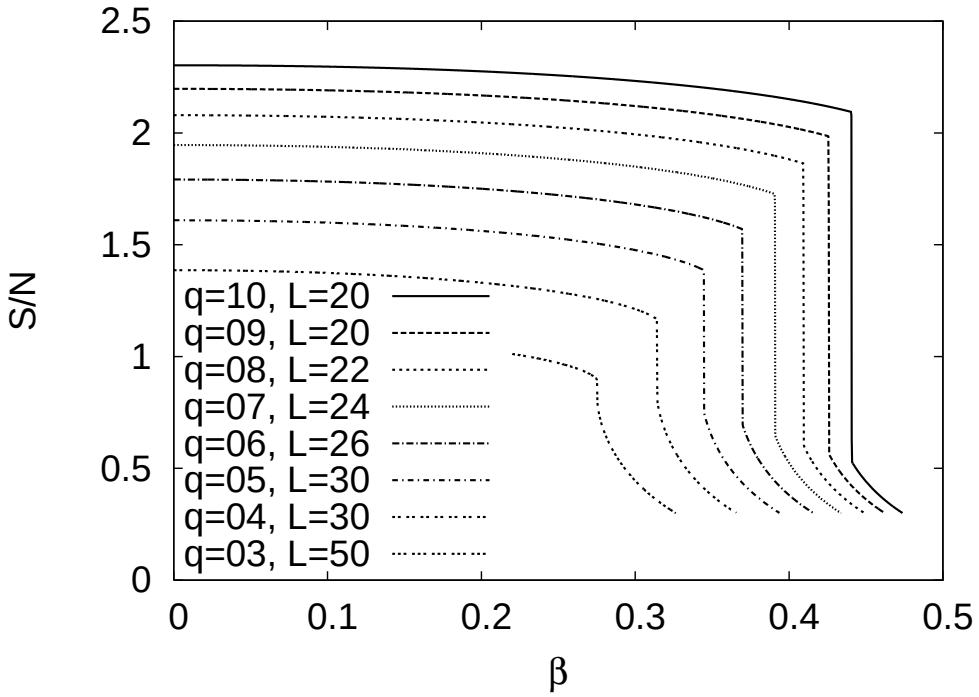

FIG. 3: Normalized entropy densities.

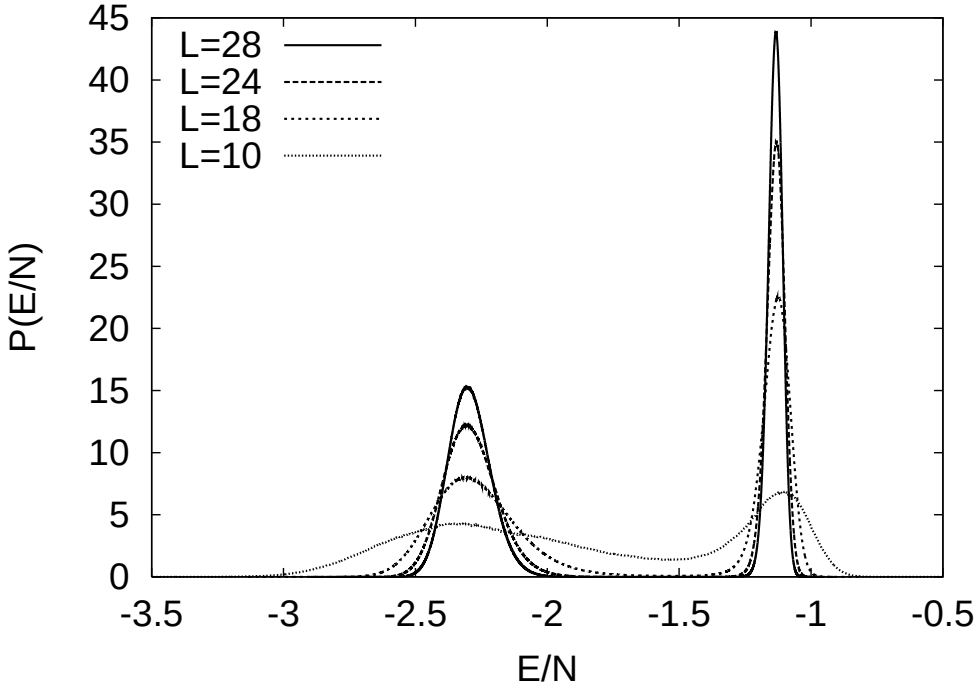

FIG. 4: Energy density histograms at $\beta_{pt}^2(L)$ for $q = 4$.

TABLE V: Estimates of observables ($q = 3$ from Ref. [18]).

q	$s(\beta_t)$	$f(\beta_t)$	s^+	s^-	w^+	w^-
2	0.55715 (31)	-3.50956 (23)	$s(\beta_t)$	$s(\beta_t)$	1.75	1.75
3	0.8491 (21)	-4.431364 (50)	0.8943 (21)	0.8038 (22)	2.45	2.24
4	0.983 (11)	-4.846358 (41)	1.166 (11)	0.800 (11)	3.21	2.23
5	1.0680 (70)	-5.084679 (34)	1.3862 (70)	0.7498 (70)	4.00	2.12
6	1.1324 (93)	-5.239933 (50)	1.5695 (93)	0.6954 (93)	4.80	2.00
7	1.1858 (85)	-5.349346 (60)	1.7262 (85)	0.6455 (85)	5.62	1.91
8	1.233 (13)	-5.430753 (66)	1.863 (13)	0.602 (13)	6.44	1.83
9	1.274 (14)	-5.493609 (42)	1.984 (14)	0.563 (14)	7.27	1.76
10	1.312 (11)	-5.543856 (50)	2.094 (11)	0.530 (11)	8.11	1.70

where $e_L^{\pm}(\beta_{pt}^2)$ are the locations of the maxima of the double peak histogram at $\beta_{pt}^2(L)$. For $q = 4$ these histograms are shown in Fig. 4 (we excluded the $L = 30$ lattice to keep a reasonable scale in the figure). This construction ensures that the energy endpoints $e_L^{\pm}$ are positioned symmetrically about the central energy density $e_L(\beta_{pt}^2)$:

$$e_L^{\pm} = e_L(\beta_{pt}^2) \pm \frac{1}{2} \triangle e_L \tag{22}$$

and one finds that

$$s_L^{\pm} = s_L(\beta_{pt}^2) \pm \frac{1}{2} \triangle s_L \tag{23}$$

holds as well. As in [18] we use jackknife estimators and arrive at the values for $e(\beta_t)$, e^+ and e^- compiled in table IV and those for $s(\beta_t)$, $f(\beta_t)$, s^+ and s^- compiled in table V. Although there are simple relations between these values, we have to list them separately, because these relations do not determine error bars. The estimates are correlated and the jackknife procedure takes care of correct error bars. Also it should be noted that β_t in the arguments of e, s and f is β_t^2, defined as the extrapolation of the pseudo transition temperatures as defined by (21). These values are consistent with the β_t values listed in table IV, but not identical, as β_t of table IV is the average of the extrapolations from our three definitions of pseudo transition temperatures.

In the last two columns of table V we give the first few digits of the effective number of states on the disordered and ordered sides of the phase transition,

$$w^{\pm} = \exp(s^{\pm}) \ . \tag{24}$$

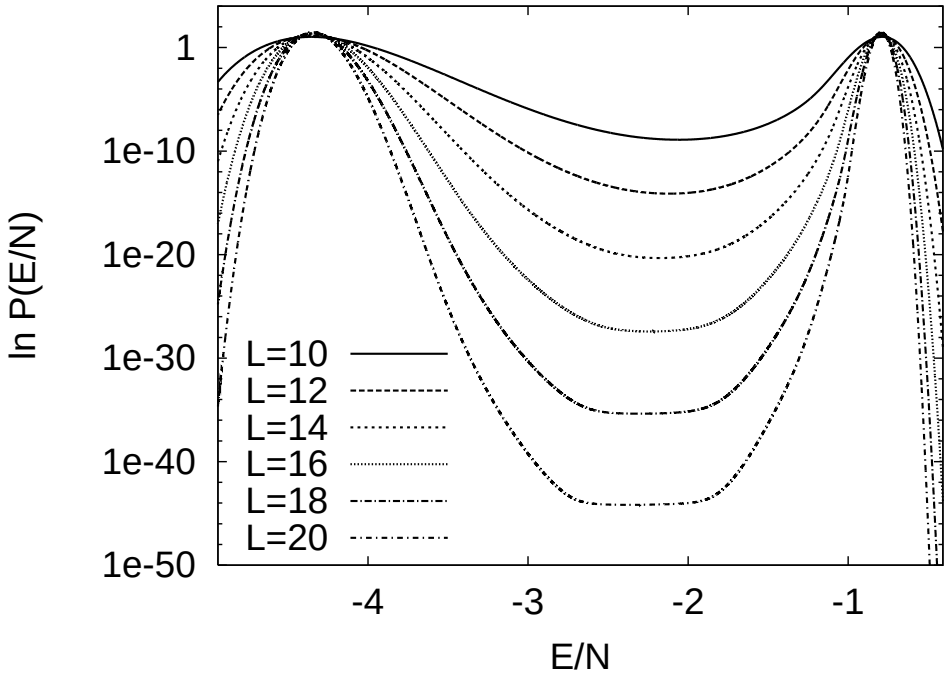

FIG. 5: Equal heights energy density histograms $q = 10$.

Amazingly, the effective number of states per spin at the the ordered endpoint goes down by increasing q.

V. INTERFACE TENSIONS AND SPINODAL ENDPOINTS

For $L \to \infty$ the interface tension between ordered and disordered phases is [29]

$$2\sigma_{od}(L) = \frac{1}{L^2} \ln \left(\frac{P_{\max}(L)}{P_{\min}(L)} \right) \tag{25}$$

where $P_{\max}(L)$ represents the value of the maxima when the energy histogram is reweighted to equal heights and $P_{\min}(L)$ the minimum in between the peaks. For $q = 10$ we show our equal heights histograms in Fig. 5. Including capillary waves [30, 31, 32], we perform 2- and 3-parameter fits to the form (compare Eq. (16) of [33])

$$2\,\sigma_{od}(L) + \frac{\ln(L)}{2L^2} = 2\sigma_{od} + \frac{c_2}{L^2} + \frac{c_3}{L^3}\ . \tag{26}$$

In case of the 2-parameter fits we set $c_3 = 0$. While the 3-parameter fits are somewhat unstable, consistent 2-parameter fits are limited to the largest three lattices. The differences between these fits exhibit systematic errors, which show that larger lattices are needed for

TABLE VI: Estimates of interface tensions (yes/no refers to capillary waves, $q = 3$ from Ref. [18]).

q	$2\,\sigma_{od}$ – yes	$2\,\sigma_{od}$ – no	q	$2\,\sigma_{od}$ – yes	$2\,\sigma_{od}$ – no
3	0.001806 (35)	0.001602 (35)	7	0.1484 (15)	0.1478 (17)
4	0.0224 (11)	0.0221 (13)	8	0.1897 (56)	0.1891 (56)
5	0.0632 (21)	0.0628 (22)	9	0.2308 (87)	0.2302 (84)
6	0.1054 (50)	0.1050 (45)	10	0.2628 (40)	0.2688 (47)

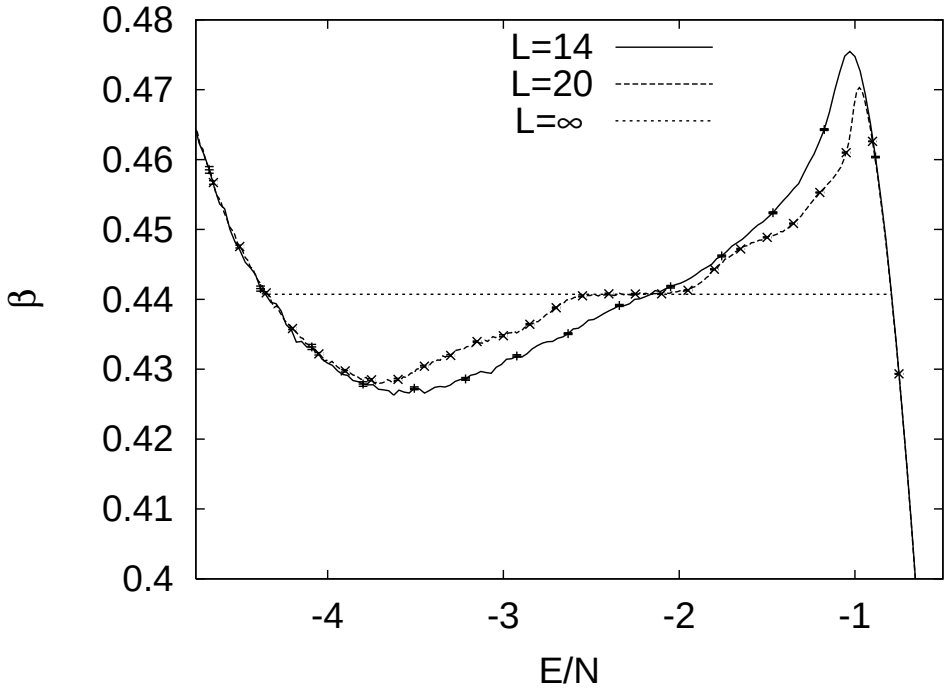

FIG. 6: Microcanonical temperature $b(E)$ for $q = 10$.

high precision results. The results of the 2-parameter fits are compiled in table VI, where the differences to the less stable 3-parameter fits are used to estimate systematic errors, which are, in these cases, substantially larger than statistical errors of the fits.

We also include in table VI results from fits without the capillary wave contribution $\ln(L)/(2L^2)$. With the exception of the $q = 3$ case from Ref. [18], the difference between the two fits is always smaller than the expected error from other sources.

The double peak histograms at first order phase transitions are intimately related to a Maxwell construction [34, 35] for the inverse microcanonical temperature $b(E)$ defined by Eq. (6). For $q = 10$ and two lattice sizes this is shown in Fig. 6. The areas above and below

the infinite volume line are identical and for $L = 20$ one sees that a small fraction of the curve joins this line.

The minimum $\beta^{\rm sp}_{\rm min}$ and the maximum $\beta^{\rm sp}_{\rm max}$ of the $\beta(E)$ curve are the inverse spinodal temperatures. Equilibration at β with dissipative model A (Glauber) dynamics [36] encounters metastability in the range $\beta_t < \beta < \beta^{\rm sp}_{\rm max}$ after a disordered start, whereas after an ordered start it encounters metastability in the range $\beta_t > \beta > \beta^{\rm sp}_{\rm min}$. For the $\beta(H)$ of a magnetic field driven phase transition [26] this would already be the entire metastability picture. In case of the temperature driven phase transitions of Potts model it is more complicated, because metastability after a disordered start persists for equilibration at $\beta > \beta^{\rm sp}_{\rm max}$ due to order-order domain walls, which are for $q = 3$ investigated in Ref. [37].

In the past there may have been some hesitation in identifying $\beta^{\rm sp}_{\rm min}$ and $\beta^{\rm sp}_{\rm max}$, as defined here, with the spinodal endpoints. The reason is that their values agree in the infinite volume limit with β_t [34, 35] as is illustrated by the dotted line in Fig. 6. So the metastability disappears in the infinite volume limit, whereas the opposite is the case for the mean field spinodal, which is introduced in many textbooks [38]. However, the recent finite volume analysis [39] of Kolmogorov-Johnson-Mehl-Avrami (KJMA) theory demonstrates that the mean field approach is a conceptually wrong starting point for describing the infinite volume limit of phase conversion. Within the KJMA framework one gets for $V \to \infty$ always spinodal decomposition [40] and never metastability. Our definitions of $\beta^{\rm sp}_{\rm min}$ and $\beta^{\rm sp}_{\rm max}$ are consistent with this picture as well as with studies of magnetic field driven phase transitions by Rikvold et al. [41].

For large L the areas in the Maxwell construction are known [35] to shrink $\sim 1/L$. Therefore, the leading order 2-parameter fit for $\beta^{\rm sp}(L)$ is

$$\beta^{\rm sp}(L) - \beta_t = \frac{a_1}{\sqrt{L}} \left(1 + \frac{a_2}{L}\right) . \tag{27}$$

Using β_t from table IV we show in Fig. 7 the fits to this form. Together with their goodness of fit Q [2] the fit parameters are collected in table VII. The Q values are a bit on the high side, as a relatively flat $\beta(E)$ curve tends to give rather large statistical errors for the spinodal estimates $\beta^{\rm sp}(L)$. In table VII this is reflected by a_2 parameters, which are mainly statistical noise about zero. For the $q = 3$ data [18], $\beta(E)$ is altogether too flat to allow for reasonably accurate $\beta^{\rm sp}(L)$ estimates (larger lattices would be needed).

VI. SUMMARY AND CONCLUSIONS

For 3D, q-state Potts models in the range $q = 4, \ldots, 10$ we have estimated a number of observables by multicanonical MCMC calculations and supplemented them with $q = 2$

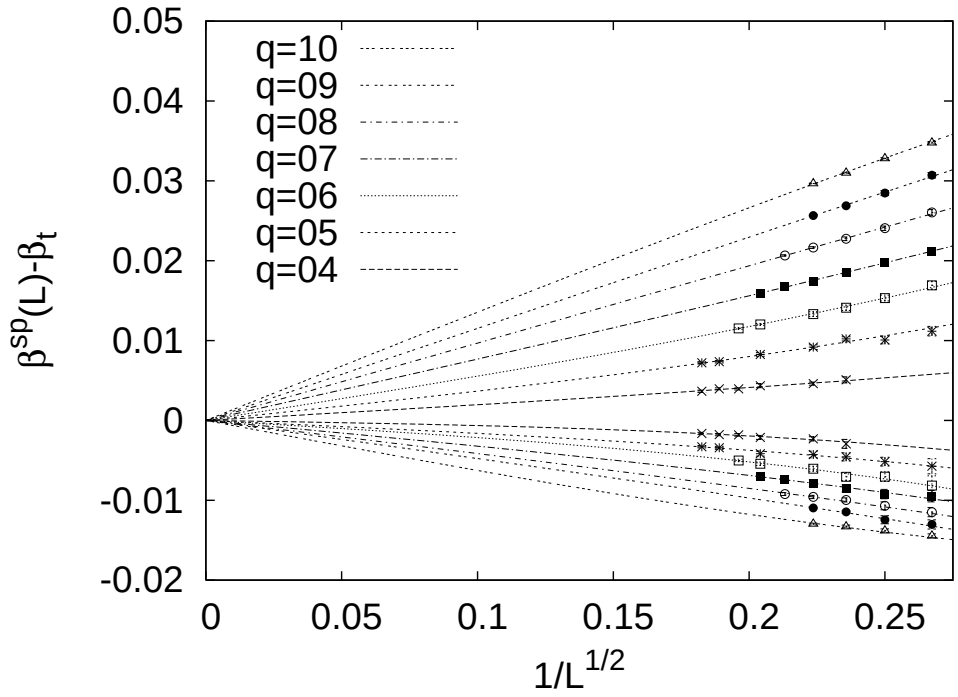

FIG. 7: FS behavior of the spinodals.

TABLE VII: Estimates of the fit parameters of Eq. (27).

q	$a_{1,\max}$	$a_{2,\max}$	Q	$a_{1,\min}$	$a_{2,\min}$	Q
4	0.0193 (21)	1.6 (3.0)	0.57	-0.0053 (24)	21 (21)	0.83
5	0.0357 (20)	3.0 (1.5)	0.19	-0.0154 (19)	5.5 (3.7)	0.84
6	0.0543 (20)	2.07 (89)	0.84	-0.0200 (29)	7.5 (4.3)	0.81
7	0.0764 (22)	0.53 (57)	0.67	-0.0315 (27)	2.3 (2.0)	0.95
8	0.0969 (10)	-0.01 (19)	0.85	-0.0412 (27)	0.8 (1.4)	0.69
9	0.1154 (19)	-0.14 (30)	0.58	-0.0475 (25)	0.6 (1.1)	0.82
10	0.13631 (93)	-0.58 (12)	0.05	-0.0639 (19)	-2.00 (41)	0.21

and $q = 3$ results from the literature. Transition temperatures, latent heats and energy endpoints of the phases are given in table IV, entropy and free energy values in table V.

Less accurate are our interface tension estimates of table VI. They could possibly be improved by using simulation techniques similar to those, which led to high-precision estimates of the order-order interface tension in the 3D Ising model [42].

Minima and maxima of the microcanonical inverse temperature curve $b(E)$ are identified

as adequate definition of spinodal endpoints. As expected [39, 41] the thus defined regions of metastability disappear in the infinite volume limit.

We hope that future investigations of 3D first order phase transitions will benefit from the results collected in this paper.

Acknowledgements: This work was in part supported by DOE grants DE-FG02-97ER-41022 and DE-FC02-06ER-41439 and by NSF grant 0555397.

---

[1] R.B. Potts, Proc. Cambridge Philos. Soc. 48 (1952) 106.

[2] B.A. Berg, *Markov Chain Monte Carlo Simulations and Their Statistical Analysis*, World Scientific, Singapore, 2004.

[3] F.Y. Wu, Rev. Mod. Phys. 54 (1982) 235.

[4] R.J. Baxter, J. Phys. C 6 (1973) L445.

[5] C. Borgs and W. Janke, J. Phys. I France 2 (1992) 2011 and references therein.

[6] B.A. Berg and T. Neuhaus, Phys. Rev. Lett. 68 (1992) 9.

[7] S.F. Edwards and P.W. Anderson, J. Phys. F 5 (1975) 965.

[8] K. Binder, *Quadrupolar Glasses and Random Fields*, in *Spin Glasses and Random Fields*, A.P. Young (editor), World Scientific, Singapore 1997.

[9] J. Villain, J. Phys. C 10 (1977) 1717.

[10] B. Svetitsky and L.G. Yaffe, Nucl. Phys. B 210 (1982) 443.

[11] R.V. Gavai, F. Karsch, and B. Petersson, Nucl. Phys. B 322 (1989) 738.

[12] M. Fukugita, H. Mino, M. Okawa, and A. Ukawa, J. Stat. Phys. 59 (1990) 1397.

[13] N. Alves, B.A. Berg and R. Villanova, Phys. Rev. B 43 (1991) 5846.

[14] M. Schmidt, Z. Phys. B 95 (1994) 327.

[15] W. Janke and R. Villanova, Nucl. Phys. B 489 (1997) 679.

[16] F. Karsch and S. Stickan, Phys. Lett. B 488 (2000) 319.

[17] R. Falcone, R. Fiore, M. Gravina, and A. Papa, Nucl. Phys. B 767 (2007) 385.

[18] A. Bazavov and B.A. Berg, Phys. Rev. D 75 (2007) 094506.

[19] A. Gendia and T. Nishino, Phys. Rev. E 65 (2002) 046702.

[20] A.K. Hartmann, Phys. Rev. Lett. 94 (2005) 050601.

[21] M. Hellmund and W. Janke, Phys. Rev. E 74 (2006) 051113.

[22] B. Hesselbo and R. Stinchcombe, Phys. Rev. Lett. 74 (1995) 2151.

[23] S. Trebst, D.A. Huse, and M. Troyer, Phys. Rev. E 70 (2004) 046701.

[24] T. Neuhaus and J.S. Hager, J. Stat. Phys. 113 (2003) 47.

[25] F. Wang and D.P. Landau, Phys. Rev. Lett. 86 (2001) 2050.

[26] B.A. Berg, U.H. Hansmann, and T. Neuhaus, Z. Phys. 90 (1993) 229.

[27] A.L. Talapov and H.W.J. Blöte, J. Phys. A: Math. Gen 29 (1996) 5727.

[28] M.S.S. Challa, D.P. Landau, and K. Binder, Phys. Rev. B 34 (1986) 1841.

[29] K. Binder, Phys. Rev. A 25 (1982) 1699.

[30] E. Brézin and J. Zinn-Justin, Nucl. Phys. B 257 (1985) 867.

[31] M.P. Gelfand and M.E. Fisher, Physica A 166 (1990) 1.

[32] J.J. Morris, J. Stat. Phys. 69 (1991) 539.

[33] A. Billoire, T. Neuhaus and B.A. Berg, Nucl. Phys. B 413 (1994) 795.

[34] A. Hüller, Z. Phys. B 95 (1994) 63.

[35] W. Janke, Nucl. Phys. B (Proc. Suppl.) 63A-C (1998) 631.

[36] R.J. Glauber, J. Math. Phys. 4 (1963) 294. Model A in the classification of P.M. Chaikin and T.C. Lubensky, *Principles of condensed matter physics*, Cambridge University Press, Cambridge 1997, Table 8.61.1, p.467.

[37] B.A. Berg, H. Meyer-Ortmann, and A. Velysky, Phys. Rev. D 70 (2004) 054505; A. Bazavov, B.A. Berg, and A. Velytsky, Phys. Rev. D 74 (2006) 014501.

[38] E.g., D.P. Landau and K. Binder, *A Guide to Monte Carlo Simulations in Statistical Physics*, Cambridge University Press 2000, p.41.

[39] B.A. Berg and S. Dubey, Phys. Rev. Lett. 100 (2008) 165792.

[40] Here we use the terminology "spinodal decomposition" in a broader sense than some statistical physicists do.

[41] P.A. Rikvold, H. Tomita, S. Miyashita, and S.W. Sides, Phys. Rev. E 49 (1994) 5080; M.A. Novotny, G. Brown, and P.A. Rikvold, J. Appl. Phys. 91 (2002) 6908.

[42] M. Caselle, M. Hasenbusch, and M. Panero, JHEP 9 (2007) 117 and references given therein.